Geophysical Research Letters

RESEARCH LETTER
10.1029/2025GL117155

Early Warming Over the Southern Ocean During the Last Deglaciation

Peisong Zheng[1,2], **Thomas Bauska**[2], **and Matthew Osman**[1]

[1]Department of Geography, University of Cambridge, Cambridge, UK, [2]British Antarctic Survey, Cambridge, UK

Key Points:

- A Gaussian Mixture Model is used to classify reanalysis and model-based climate reconstructions of the last deglaciation
- Among four distinct temperature classes identified, the Southern Hemisphere high latitudes warmed earliest, at around 21,000 years ago
- Weakening of the Atlantic Meridional Overturning Circulation, driven by orbital forcing, is likely the cause of this early warming

Supporting Information:

Supporting Information may be found in the online version of this article.

Correspondence to:

P. Zheng,
pz285@cam.ac.uk

Citation:

Zheng, P., Bauska, T., & Osman, M. (2025). Early warming over the southern ocean during the last deglaciation. *Geophysical Research Letters*, *52*, e2025GL117155. https://doi.org/10.1029/2025GL117155

Received 22 MAY 2025
Accepted 20 AUG 2025

Author Contributions:

Conceptualization: Peisong Zheng
Formal analysis: Peisong Zheng
Funding acquisition: Peisong Zheng
Methodology: Peisong Zheng, Thomas Bauska, Matthew Osman
Project administration: Thomas Bauska, Matthew Osman
Resources: Matthew Osman
Software: Peisong Zheng, Matthew Osman
Supervision: Thomas Bauska, Matthew Osman
Validation: Peisong Zheng, Matthew Osman
Visualization: Peisong Zheng, Thomas Bauska, Matthew Osman
Writing – original draft: Peisong Zheng

Abstract The last deglaciation, ca. 17,000–11,000 years before present (yr BP), marks the most recent period of large-scale climate reorganization on Earth. However, the timing and spatial patterns of the initial warming preceding these changes remain uncertain. Here, we develop a new method using Gaussian Mixture Model clustering to objectively segregate a reanalysis and climate model simulations, respectively, into four distinct patterns of temperature change throughout the last deglaciation. Our findings indicate that the earliest warming signs appeared around 21,000 years BP in the Southern Hemisphere high latitudes. This early warming was accompanied by a cooling in the Northern Hemisphere high latitudes, resulting in a hemispherically asymmetric temperature pattern. Further analysis using single-forcing climate simulations suggests that the early warming and sea ice retreat were likely driven by a weakening in the Atlantic Meridional Overturning Circulation, linked to orbital forcing.

Plain Language Summary Perhaps the most significant recent climate change event is the transition from the last ice age (ca. 21,000–19,000 years ago). This transition took several thousand years and invoked significant changes upon almost every aspect of the climate system. While small changes in Earth's orbit around the Sun were the primary trigger, the mechanisms through which the climate system responded to, and ultimately brought about, these changes are still uncertain. By adapting a type of statistical learning model used to understand clustering in large data sets, we found that the Southern Ocean was the first region to warm as the world emerged from the last ice age. Further analysis suggests this early warming was likely linked to a slowing Atlantic ocean circulation, itself driven by changes in sunlight reaching the Northern Hemisphere high latitudes.

1. Introduction

Past periods of climate change provide valuable analogs for the processes shaping today's warming world. The most recent large-magnitude natural warming was the last deglaciation, when Earth's climate transitioned from a cold glacial state to a warm interglacial one. This period was characterized by significant climatic shifts, including a ~6–7°C rise in global mean temperature (Clark et al., 2024; Osman et al., 2021; Seltzer et al., 2021; Tierney et al., 2020), a mean global sea-level increase of about 130 m (Spratt & Lisiecki, 2016), and an increase in atmospheric CO_2 levels of about 80 ppm (Bereiter et al., 2015; Marcott et al., 2014). On a globally averaged basis, the major warming of the last deglaciation occurred between ca. 17,000 and 8,000 years BP (the present is defined as 1950 CE) according to a global mean surface temperature reconstruction (Osman et al., 2021). Nonetheless, questions surrounding which region(s) warmed first and why remain topics of ongoing debate.

Growing model-based evidence suggests that the earliest warming of the last deglaciation may have begun over Southern Hemisphere high latitudes as early as 20,000–22,000 years BP (He et al., 2013; Sadatzki et al., 2023; Timmermann et al., 2009). The drivers of this early warming have been attributed to various factors, including a weakening of the Atlantic Meridional Overturning Circulation (AMOC) (Obase et al., 2023); feedbacks reflecting local insolation forcing such as integrated summer energy (Huybers, 2006), peak summer insolation (Collins et al., 2012; van den Bos et al., 2018; WAIS Divide Project Members, 2013), or spring insolation (Stott et al., 2007); and a diminishing of Southern Ocean sea ice and an associated shift in westerly winds (Menviel et al., 2018; Obase et al., 2023). To date, no study has produced a quantitative, spatially explicit map identifying the onset of deglacial warming across regions while also separating the contributions of the various climate modes driving those differences.

Global proxy compilations have similarly shed some light on the early warming. Shakun and Carlson (2010) first conducted an analysis of climate dynamics during the last deglaciation by compiling global temperature proxy records (Shakun & Carlson, 2010; Shakun et al., 2012). These authors demonstrated that the Southern Ocean and

Writing – review & editing: Peisong Zheng, Thomas Bauska, Matthew Osman

Antarctica warmed approximately between 19,000 and 17,500 years BP (Cuffey et al., 2016; Shakun & Carlson, 2010; Shakun et al., 2012; WAIS Divide Project Members, 2013). More recently, the Last Glacial Maximum Reanalysis (LGMR) data set has been developed using a data assimilation technique that combines a model-based (CESM1.2 and 1.3) temperature reconstruction with an extensive proxy data set to form a global-scale reanalysis covering the past 24,000 years (Osman et al., 2021). Similar to prior studies (Shakun et al., 2012), two Principal Components (PCs) were identified. The first PC (PC1) of the LGMR was found to be broadly reflective of combined changes in greenhouse gases and ice sheets, implying a mild global cooling trend prior to ∼17,000 years BP. On the other hand, the second PC (PC2)—a "bipolar" hemispheric mode reflecting millennial-scale variability superimposed on slower-moving orbital changes—indicated a much earlier warming across the Southern Ocean (Osman et al., 2021) (Figure S1 in Supporting Information S1). However, a precise attribution of the regional importance of this mode relative to PC1 was not clearly identified through such analysis.

In this study, we investigate the initiation of the last deglaciation and the early Southern Ocean warming using an unsupervised clustering method based on the Gaussian Mixture Model (GMM), to classify LGMR- and climate model-derived time series based on their contribution to the PCs. This method enables us to identify the spatial boundaries of regions with significantly different deglacial warming signatures, but also aids in partitioning the onset timing of the last deglaciation differentially across space. Our study is outlined as follows: First, we apply our GMM classification algorithm to the LGMR data assimilation product to deconvolve the complex spatial and temporal patterns of deglaciation temperature change into four major classes. Next, we apply a Bayesian change point detection method to determine the timing of earliest warming in each class. Finally, we speculate on the possible drivers of the earliest phase of the last deglaciation using climate model factorial experiments.

2. Methods

The GMM approximates the joint distribution of surface air temperature (SAT) trajectories at each LGMR grid point by representing it as a weighted sum of K multivariate Gaussian components in PC space (Boland et al., 2023; Xuan et al., 2001). As an unsupervised learning method, it enables the identification of sub-populations without requiring prior knowledge of their group membership. For a data set with N grid points, where each grid point is a SAT time series, the joint probability distribution is given by Dempster et al. (1977):

$$p(x) = \sum_{i=1}^{K} \phi_i \mathcal{N}(x|\mu_i, \Sigma_i) \tag{1}$$

Here, $\mathcal{N}(x\,|\,\mu_i, \Sigma_i)$ represents a multivariate Gaussian distribution with mean μ_i and covariance matrix Σ_i (Boland et al., 2023; Xuan et al., 2001):

$$\mathcal{N}(x|\mu_i, \Sigma_i) = \frac{1}{\sqrt{(2\pi)^k |\Sigma_i|}} \exp\left(-\frac{1}{2}(x-\mu_i)^{\mathrm{T}} \Sigma_i^{-1} (x-\mu_i)\right), \tag{2}$$

such that the mixing coefficients ϕ_i satisfy:

$$\sum_{i=1}^{K} \phi_i = 1, \quad \phi_i \in [0, 1]. \tag{3}$$

Then, an expectation-maximization algorithm is used to iteratively maximize the log-likelihood and estimate the means and standard deviations of the Gaussian distributions (D. C. Jones et al., 2019). The class with the highest probability is subsequently assigned as the class label for each LGMR data point. Here we use the GMM function from the `scikit-learn` Python package (version 1.2.2, Pedregosa et al., 2011). For more discussion on the details of the method and its applications in earth science, please refer to previous research (Boland et al., 2023; D. C. Jones et al., 2019).

We focus our study around the deglacial interval spanning 24,000 to 11,000 years BP in order to exclusively examine temperature changes during the pre-deglaciation and deglaciation phases; this period includes both the

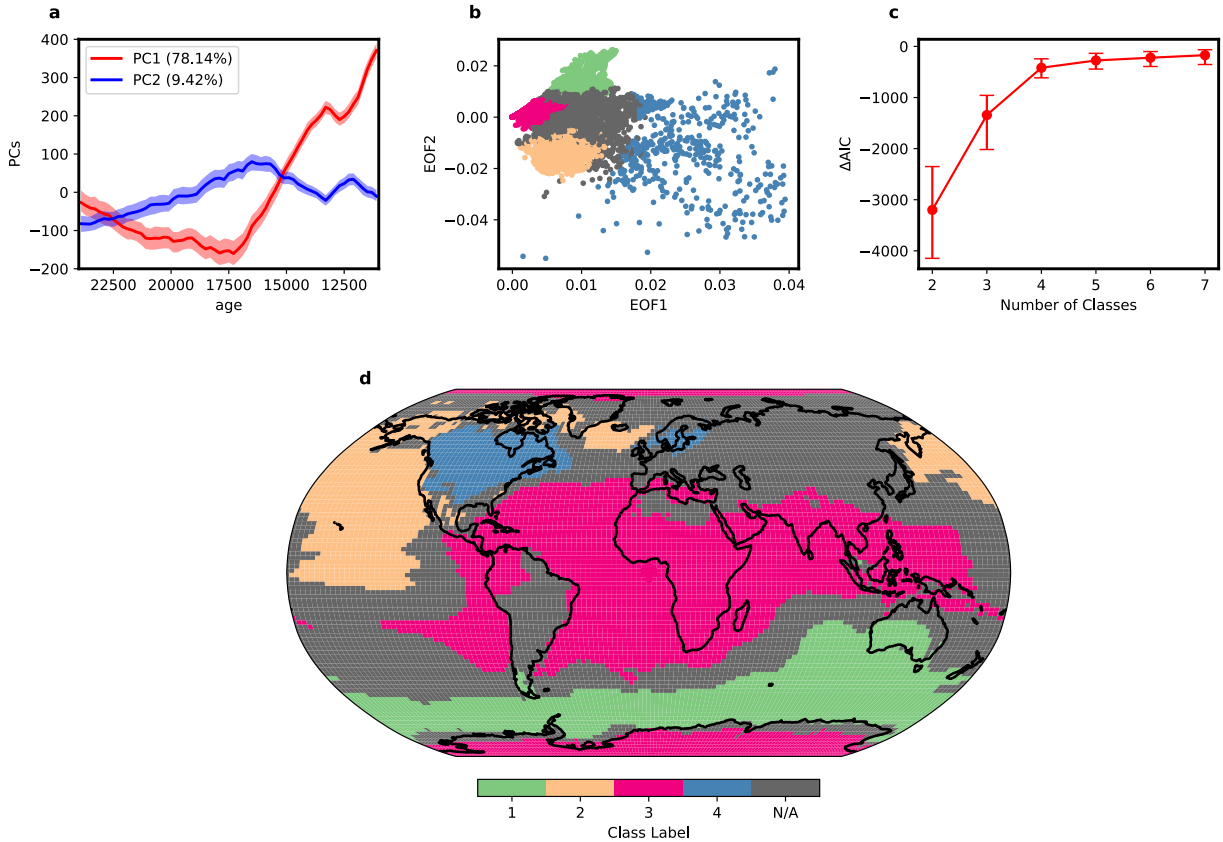

Figure 1. Gaussian Mixture Model (GMM) classification of the Last Glacial Maximum Reanalysis (LGMR). (a) The first and second Principal Components (PCs) of the LGMR (Osman et al., 2021), with thick lines indicating the mean of the data and light shading the interquartile ranges ($n = 500$). (b) The scatter plot of the corresponding Empirical Orthogonal Functions (EOFs) of the LGMR, with the classes assigned by the GMM separated by colors. Data points with <90% consistency are marked by gray (see Supporting Information S1). (c) The ΔAkaike Information Criterion (ΔAIC; error bars mark the interquartile ranges across the LGMR ensemble). (d) The spatial distribution of class labels from panel (b).

major millennial-scale climate events (i.e., Heinrich Stadial 1 (HS1), the Bølling–Allerød (BA), and Younger Dryas (YD); Figure 1) as well as adequate coverage of the pre-deglacial (i.e., glacial) state. Using the LGMR data set, we perform Principal Component Analysis following the method described by Osman et al. (2021) across the 500 member ensemble; this reduces the data dimensionality ahead of the GMM classification by retaining only the first two PCs, which explain, on average, 78.14% and 9.42% of data variance, respectively (Figure 1a). We then classify each temperature series according to its position in Empirical Orthogonal Function (EOF) space, which reflects that series' contribution to the principal components (Figure 1b, Figure S1 in Supporting Information S1). This approach highlights regions exhibiting pronounced early warming, as reflected in PC2, and helps isolate the dominant global temperature modes of the last deglaciation according to their association with the two governing climate trends represented by the PCs.

The sole free parameter of the GMM is the number of mixture components, K. We selected K by minimizing the Akaike Information Criterion (AIC, Supporting Information S1) for $K = 2$–8, using the ensemble-mean principal components as input (Figure 1c (Akaike, 1973)). The ΔAIC confirms that improvements beyond $K = 4$ are statistically marginal ($p < 0.01$; Boland et al., 2023). Sensitivity tests with $K = 3$–6 on the LGMR ensemble mean (Figure S2 in Supporting Information S1) reinforce this choice. When $K = 5$, the fifth component overlaps almost entirely with the grid cells that already display high classification uncertainty in Figure 1d, adding little dynamical information. Also, for $K > 4$, additional components simply partition the interiors of the four clusters listed above, a hallmark of over-fitting (Boland et al., 2023). Thus, $K = 4$ provides the most parsimonious yet physically meaningful representation of the deglacial SAT field.

Since class labels are assigned randomly for each ensemble member by the GMM, we used the mean LGMR-inferred class labels as a reference point for realigning classes from the full ensemble based on an index of maximum overlap. The spatial distribution of class labels, along with the uncertainty of the classification (Supporting Information S1), is shown in Figure 1d. A similar spatial pattern is also found in the Transient Climate Evolution (TraCE) climate simulation (He et al. (2013); Figures 2a–2d), with differences discussed in Supporting Information S1. This data set features a previous-generation, and lower-resolution, climate model (CCSM3) than that used to develop the LGMR (CESM1.2 and 1.3), and is also independent of surface temperature-related proxy data. The latest TraCE simulation, TraCE–21K–II—which revises the meltwater forcings but retains the same orbital, greenhouse-gas and ice-sheet boundary conditions as its predecessor—yields deglacial classifications that are virtually indistinguishable from the original TraCE simulation (He et al., 2022, Figure S3 in Supporting Information S1).

Several methodological caveats warrant acknowledgment. First, the Gaussian Mixture framework constrains each cluster to an elliptical, multivariate-normal distribution (Boland et al., 2023), whereas empirical paleotemperature fields often exhibit heavy tails, skewness, or multimodality; such departures from normality can bias the estimated responsibilities and blur class boundaries. Second, representing the continuous spectrum of climate variability with a finite set of mixture components inevitably sacrifices spatial nuance. While increasing the number of classes reveals additional physically plausible sub-regions (Figure S2 in Supporting Information S1), our classification choice reflects a trade-off between interpretability and parsimony on a global basis, in order to emphasize large-scale modes. Finally, as highlighted by Ye and Zhou (2025), the posterior probabilities of the GMM applied to spatio-temporal data grids systematically decline in dynamically complex zones, indicating reduced robustness and effective spatial resolution of the classification in these regions (Figure S4 in Supporting Information S1).

3. Results

The four classes identified by the GMM correspond to several known climate patterns of the last deglaciation. Class 4 is, broadly speaking, the "ice sheet class": it exhibits the highest amplitude of deglacial warming (more than 15°C, Figures 1 and 2d) and encompasses the ice sheet regions of North America and Europe (Figure 1d) (Clark et al., 2009), suggesting that it is dominated by an ice-sheet—controlled feedbacks: namely, ice-albedo and lapse-rate temperature-related processes. Class 4 shows the strongest skew across all four classes in the PC1 versus PC2 projection plot (Figure 1b), suggesting a less specific influence from climate processes behind PC1 and PC2, respectively. We applied a Bayesian change point detection method to each class's area-weighted average temperature time series (Figure 2) to identify the onset of deglacial warming by detecting when the trend shifted from cooling to warming (using Python package BEAST version 1.1.2.60, Li et al. (2022), Zhao et al. (2019), Supporting Information S1). The initiation of the last deglaciation for this class is estimated as 16,890 years BP (95% Confidence Interval (CI): 17,140 to 16,650 years BP).

The class-mean trajectories of Class 4 (and the other three classes) derived from TraCE (Figure 2d) exhibit more pronounced abrupt features, especially during the BA interval, than those from LGMR. This is partly due to the higher temporal resolution of TraCE and the idealized character of its prescribed meltwater forcing, which enhances AMOC variability and amplifies inter-hemispheric contrasts (He et al., 2013). The LGMR, in turn, is smoothed both by its 200-year temporal resolution and by age uncertainties in the proxy data, both of which likely dampen the expression of abrupt events.

Class 2 includes the North Pacific, tropical and subtropical West Pacific, and North Atlantic (Figures 1d and 2b). This class, which we term the "northern seat of the bipolar seesaw", imprints most negatively upon PC2 and largely reflects those regions that were subjected to strong cooling during intervals of elevated Atlantic and Pacific freshwater forcing during the early (18,000 to 16,500 years BP) and late (16,400 to 15,000 years BP) HS1 intervals, and during the YD (ca. 12,900 to 11,700 years BP). The much stronger spatial imprint of Class 2 across the Pacific basin is consistent with emerging research suggesting a strong Pacific influence on Northern Hemisphere cooling during HS1 and the YD, likely driven by Columbia River outburst megaflooding into the North Pacific (Praetorius et al., 2020). These floods both preceded and were more abrupt than subsequent intervals of North Atlantic ice rafting and freshwater forcing (Praetorius et al., 2020; Praetorius & Mix, 2014). The deglacial onset of this class spans from 17,360 to 16,810 years BP (95% CI).

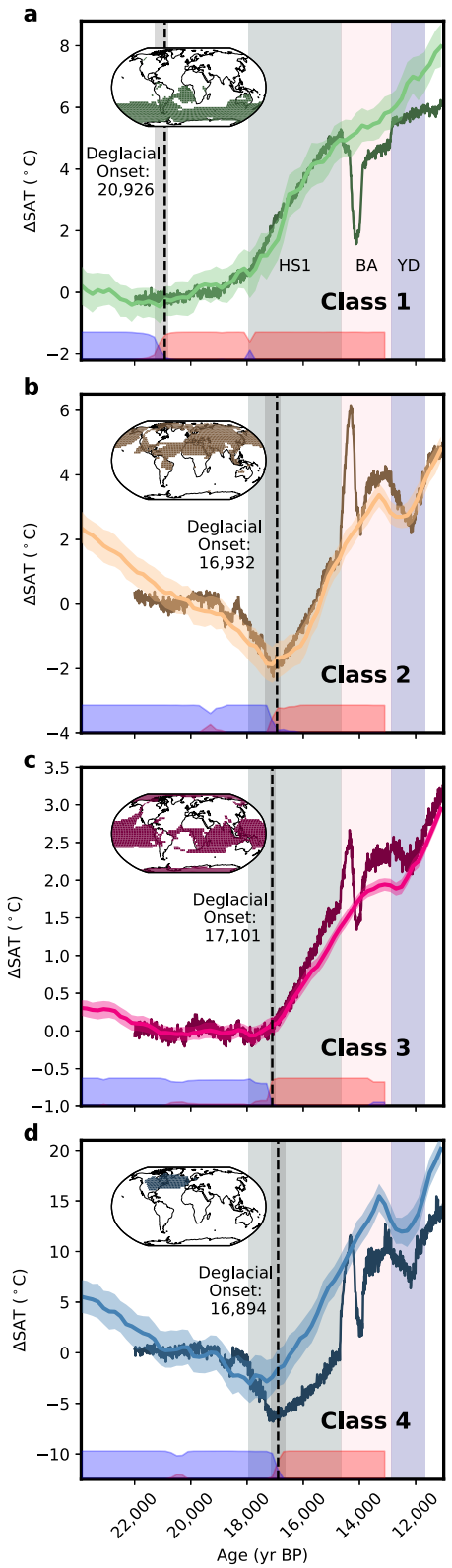

Figure 2.

The climatic origins of Class 3, covering broad swaths of the tropics, central Antarctica and even the northern-most Arctic, are more ambiguous (Figures 1d, 2b, and 2c). This class loads positively atop PC1 with no obvious systematic influence from PC2, implying a predominant influence from greenhouse gases and global-scale albedo changes (Osman et al., 2021). However, its main tropical footprint could be interpreted as the "pivot point" of the bipolar seesaw, although the inclusion of high-polar regions is not easily reconciled with that view. The comparatively low posterior probabilities assigned to this class, relative to the other classes (Figure S4 in Supporting Information S1), suggest that its underlying dynamics are sufficiently complex to challenge confident GMM classification (Ye & Zhou, 2025). The deglacial warming of this class begins between 17,190 and 17,010 years BP.

Classes 2, 3, and 4 exhibit relatively late deglacial warming that aligns with the onset of HS1 (Figure 2), suggesting their warming was primarily driven by AMOC-induced interhemispheric heat redistribution or globally uniform CO_2 forcing. All three classes show a gradual cooling trend prior to the onset of deglaciation, which likely reflects their dominant response to PC1—representing the background glacial cooling—rather than to the early warming mechanisms captured by PC2. Indeed, these classes are characterized by positive loadings on PC1 and near-zero or negative loadings on PC2 (Figure 1b), which suppress the expression of early warming encoded in PC2.

Class 1 encompasses most of Oceania and the high-latitude Southern Ocean (Figures 1d and 2a). It is the counterpart to Class 2 because it leaves a positive imprint on PC2 and represents the "southern seat" of the bipolar seesaw (Figure 1b). The robustness of this class is demonstrated by the fact that only minor subdivision occurs when the number of classes is increased (Figure S2 in Supporting Information S1). The most notable feature of this class is the large warming that occurs after 18,000 years BP (1.01°C/kiloyear, $p < 0.05$) which coincides with the start of HS1 and thus likely represents the Southern imprint of the bipolar seesaw (Barker et al., 2009; Denton et al., 2010; Wolff et al., 2009). However, this is not the onset of warming: rather, our Bayesian change point detection shows an early and gradual warming begins between 21,270 and 20,810 years BP (Figure 2a). This early warming is also observed when using an alternative change-point detection method, Significant ZERo crossings of derivatives (SiZer; Chaudhuri & Marron, 1999), which suggests that the change points of Class 1 lead those of the other classes significantly ($p < 0.05$; see Figure S5 in Supporting Information S1). A complementary sliding-window test shows that, although class boundaries can shift modestly through time, the centers of the four clusters remain near-stationary across the last deglaciation with Class 1 persistently emerging as the earliest-warming region (see Supporting Information S1).

Figure 2. Evolution of deglacial Surface Air Temperature (SAT), and initiation of deglacial warming for the Southern Ocean class. (a) The southern seat of the bipolar seesaw, (b) the northern seat of the bipolar seesaw, (c) the greenhouse gases class, (d) and the ice sheet class. The thick colored lines and light-colored shadings represent the median and the interquartile range, respectively, of each LGMR class across the full ensemble. The dark-colored curves show the GMM classes derived from the Transient Climate Evolution (TraCE) simulation, with their spatial extents indicated on the inset maps (He et al., 2013). The TraCE data has been scaled with a factor of 1.6 for comparison following previous research (Osman et al., 2021). The deglacial onset is indicated by dashed lines, along with its 95% confidence interval (gray). The red and blue shading at the bottom indicates the probabilities of the curve's trend being positive or negative, respectively (Hu et al., 2021; Zhao et al., 2013, 2019).

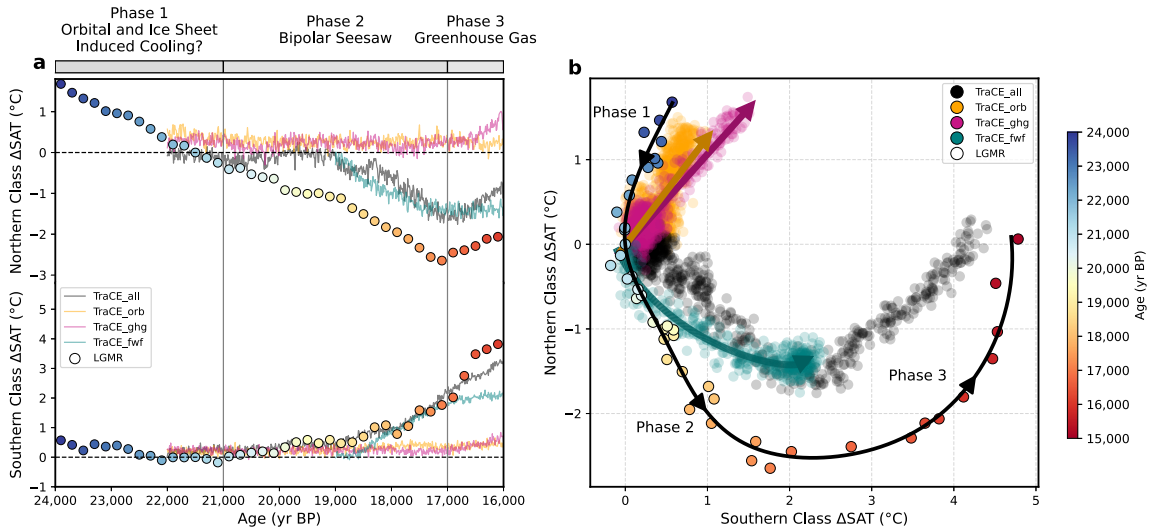

Figure 3. Fingerprints of the early deglacial warming. (a) Time series of LGMR (Osman et al., 2021) and TraCE experiments (He et al., 2013) for the Northern (upper panel, Class 2) and Southern (lower panel, Class 1) class of the bipolar seesaw. TraCE experiments include: all-forcing (all), orbital forcing (orb), greenhouse gases (ghg) forcing, and freshwater forcing: (fwf). The LGMR data points are color-coded according to their respective times. (b) Cross-plot between the Southern and Northern classes for the period 24,000 to 15,000 years BP. The black curve with arrows indicates the evolution of the LGMR data. The colored arrows represent the trends of the TraCE experiments from 22,000 to 15,000 years BP, except for the "orb" experiment, which shows the trend from 22,000 to 11,000 years BP. We sampled the TraCE temperature data corresponding spatially to the LGMR classes for direct comparison.

This early deglacial onset in Class 1 broadly aligns with the early warming inferred from the West Antarctic Ice Sheet (WAIS) Divide ice core in West Antarctica (WAIS Divide Project Members, 2013), which was not assimilated into the LGMR. The WAIS water isotope ($\delta^{18}O$) record shows a notably stronger early warming in West Antarctica compared with East Antarctica, with a 2.2‰ increase in $\delta^{18}O$ (WAIS Divide Project Members, 2013) (~2.4°C warming) between 22,000 and 18,000 years BP (Cuffey et al., 2016). Although the water isotope record at WAIS Divide has been interpreted primarily as a surface temperature signal, it is also heavily influenced by sea-ice concentration and surface temperature conditions extending as far as the mid-latitudes of the Pacific (T. R. Jones et al., 2018). The early warming recorded at WAIS is thus broadly consistent with our GMM Class 1, suggesting that the LGMR may underestimate teleconnections between Southern Ocean climate variability and Antarctic precipitation (Osman et al., 2021). In turn, our Class 1 disagrees with previous proxy data compilations (Shakun & Carlson, 2010) that suggest a Southern Ocean deglacial warming onset at ~19,000 years BP, instead indicating an earlier initiation. A detailed comparison of our findings with earlier transient-climate modeling studies that address the timing and spatial manifestations of deglacial warming (Obase et al., 2023; Roche et al., 2011; Snoll et al., 2024) is presented in Supporting Information S1.

With the timing and spatial extent of the early deglacial warming identified, we can now examine the climatological factors driving this warming onset. One key feature of the early Southern Ocean warming (Class 1) is its opposing trend relative to the Northern Hemisphere mid-to-high latitudes (Class 2; Figures 2 and 3a). The evolution of this inter-hemispheric temperature trend can be clearly delineated using a "Phase Space" diagram, as shown in Figure 3b, where we plot the LGMR Class 1 (the "southern seat" of the bipolar seesaw) against Class 2 (the "northern seat") (Figure 3b) in combination with the TraCE factorial experiment (Figure 3b, Figure S6 in Supporting Information S1). Here, we also analyze three single-forcing TraCE simulations (He et al., 2013): an insolation-only run and a greenhouse-gas-only run, both spanning 22,000–0 years BP, and a freshwater-flux run spanning 19,000–0 years BP, with all other non-target boundary conditions held fixed following He et al. (2013). The idea of using such "cross plots" to discern the mechanism of the last deglaciation under individual forcings was also implicitly explored by Gregoire et al. (2015) and Obase et al. (2023).

This bivariate representation provides insight into both the paired magnitude of inter-hemispheric temperature changes across the deglaciation, and also their joint-trajectories. Furthermore, the phase space plot provides a straightforward means of identifying the mechanistic fingerprints of early warming (He et al., 2013). Under greenhouse gas forcing alone, Classes 1 and 2 warm simultaneously (Figure 3b). Orbital changes similarly induce

symmetric warming, though their impact remains marginal when Class 1 begins to warm (Figure S6 in Supporting Information S1). In contrast, the freshwater forcing experiments, which have a weakened AMOC (He et al., 2013), reveal a strong negative correlation between Classes 1 and 2 (Figure 3b). (Note that we excluded the single forcing experiment involving ice sheets, as our northern and southern signals showed no systematic relationship (Figure S6 in Supporting Information S1); their timing and magnitude are controlled almost entirely by prescribed ice sheet mask changes).

Using these decomposed, TraCE-derived fingerprints, we assigned LGMR-inferred changes into three chronologically distinct phases (Figure 3b): In Phase 1 (ca. ∼24,000 to 21,000 years BP), both northern and southern classes show cooling trends, reflecting the continuation of global-scale cooling (Osman et al., 2021), probably in response to ice sheet expansion (Clark et al., 2009; Spratt & Lisiecki, 2016). In Phase 2, ∼21,000 to 17,000 years BP, a clear bipolar seesaw signature emerges, as characterized by the negative correlation between northern and southern classes (Figure 3b). In Phase 3 (ca. 17,000 years BP onward), both classes indicate that greenhouse gas feedbacks increasingly dominate, driving CO_2-induced global warming (Figure 3b). The distinct breakpoint, or kink, in the TraCE "all-forcing" phase space plot at around 17,000 years BP corresponds to the onset of this dominant greenhouse gas forcing.

4. Discussion

What is the driver of the early Southern Ocean deglacial warming observed in Class 1? TraCE experiments suggest that a weakened AMOC induced by freshwater forcing can effectively explain the early warming signal observed during Phase 2. Proxy records, such as $\delta^{13}C$, ϵNd, $^{231}Pa/^{230}Th$, $\delta^{18}O$ of benthic foraminifera, and $\Delta^{14}C$, trace water mass distributions and circulation strength (Böhm et al., 2015; Henry et al., 2016; Liu, 2023), but yield conflicting views of AMOC during the Last Glacial Maximum (LGM, 22,000 to 19,000 years BP), spanning a more vigorous but shallower circulation (Böhm et al., 2015) to significantly reduced transport strength (Henry et al., 2016). These non-unique interpretations stem from spatiotemporal sampling limitations and uncertainties in AMOC geometry and Antarctic Bottom Water transport (Gu et al., 2020; Pöppelmeier et al., 2022). More recently, Pöppelmeier et al. (2023) used multi-proxy-constrained Earth system model simulations to examine AMOC behavior under LGM boundary conditions. Although not specifically addressing the timing of AMOC changes or their Southern Hemisphere impacts, they found a 15%–28% reduction in deepwater formation and a 28%–44% weakening in circulation strength (Pöppelmeier et al., 2023). Ostensibly, this reduced AMOC could induce warming in the Southern Ocean with a ∼200 years delay, consistent with processes observed during Dansgaard-Oeschger events (Obase et al., 2023; Pedro et al., 2018).

The causes for a weakened AMOC at deglacial onset present a relevant avenue for future research (Barker et al., 2025). Models suggest even a small freshwater flux (∼0.02 Sv) from the Fennoscandian ice sheet to the North Atlantic could explain the weakened AMOC at LGM boundary conditions (Obase et al., 2023). Statistical analyses of proxy data, in turn, suggest that ice-age terminations align with increased Northern Hemisphere seasonality driven by decreasing precession and rising obliquity (Abe-Ouchi et al., 2013; Barker et al., 2025; Hobart et al., 2023; Huybers, 2011; Wu et al., 2020), implying the same orbital parameters that lead to ice sheet collapse must also be fundamentally linked to enhanced ice-sheet-generated freshwater flux. Additionally, decreasing precession during early warming might modulate AMOC strength through internal climate feedbacks (Shakun et al., 2012), for example, by enhancing net precipitation over the subtropical North Atlantic, lowering the salinity of the AMOC's upper branch and thereby hampering overturning (Zhang et al., 2021).

The role of local solar insolation in driving the early deglacial warming observed in Southern Hemisphere high latitudes remains uncertain (Collins et al., 2012; Sadatzki et al., 2023; Timmermann et al., 2009; WAIS Divide Project Members, 2013). TraCE simulations show that orbital forcing alone produces little to no warming in these regions (He et al., 2013; Figure 3a), though this muted response could reflect the more extensive Southern Ocean sea ice the model simulates, which would suppress insolation-induced warming impacts (Obase et al., 2023). Conversely, previous proxy and climate modeling studies suggest Southern Ocean sea-ice and temperature variations closely follow changes in obliquity (Sadatzki et al., 2023; Wu et al., 2020), and the timing of the observed early warming aligns with the rising phase of obliquity starting around 29,000 years BP (Laskar et al., 2004). Thus, while not dominant, a contribution from local insolation to the early deglacial warming in Class 1 cannot be entirely excluded.

5. Conclusions

Determining where and when the last deglaciation initiated and understanding their driving mechanisms are crucial for unraveling the processes behind one of the largest natural climate oscillations: the termination of ice ages. In this study, we used the GMM to classify global temperature changes of the last deglacial temperature variability. We identified four distinct classes based on their contributions to the two PCs, indicating that the high latitudes of the Southern Hemisphere began warming at approximately 21,000 years BP. The GMM method further allows us to delineate the spatial boundaries of the region with significant early warming.

Previous works suggest that deglacial warming at high latitudes in the Southern Hemisphere is caused by a weakened AMOC, occurring at approximately 18,000 years BP due to iceberg discharge (Denton et al., 2010; Wolff et al., 2009) or a more gradual bipolar seesaw response starting around 19,000 years BP (He et al., 2013; Shakun et al., 2012). We propose that such a weakened AMOC-induced early warming happened much earlier, around 21,000 years BP. Uncertainties remain as to whether the weakened AMOC at that time was due to freshwater discharge into the North Atlantic from ice sheets, driven by a precession minimum and rising obliquity (Barker et al., 2009, 2025; Denton et al., 2010; Obase et al., 2023), or decreasing precession-induced internal climate feedbacks (Menviel et al., 2018; Zhang et al., 2021). In either case, orbital forcings cannot be wholly dissociated as a driving factor (Barker et al., 2025; Barker & Knorr, 2021). The timing and spatial manifestation of the early Southern Ocean warming helps disentangle the interplay between orbital forcing at Northern Hemisphere high latitudes and associated feedbacks in the Earth's climate system.

Acronyms

AIC	Akaike Information Criterion
AMOC	Atlantic Meridional Overturning Circulation
BA	Bølling-Allerød
BP	Before Present (reference year 1950)
EOF	Empirical Orthogonal Functions
GMM	Gaussian Mixture Model
HS1	Heinrich Stadial 1
LGM	Last Glacial Maximum
LGMR	Last Glacial Maximum Reanalysis
PC	Principal Component
SAT	Surface Air Temperature
TraCE	Transient Climate Evolution
YD	Younger Dryas

Conflict of Interest

The authors declare no conflicts of interest relevant to this study.

Data Availability Statement

The data on which this article is based are available in Osman et al. (2021) (https://www.nature.com/articles/s41586-021-03984-4), He et al. (2013) (https://www.nature.com/articles/nature11822), and He and Clark (2022) (https://www.nature.com/articles/s41558-022-01328-2). scikit-learn 1.2.2 is available in Pedregosa et al. (2011) (https://pypi.org/project/scikit-learn/1.2.2/). BEAST 1.1.2.60 is available in Li et al. (2022) (https://github.com/

zhaokg/Rbeast). The code of this research is available on https://github.com/Peisong-Zheng/Last_deglaciation/tree/public-release.

Acknowledgments
This work was supported by the UKRI Centre for Doctoral Training in Application of Artificial Intelligence to the study of Environmental Risks (reference EP/S022961/1). P. Z. designed the research and analyzed the data; T. B. proposed interpretations for the observed classes and the early warming; M.O. designed figures and provided extensive editorial contributions. All authors participated in the analysis design, and manuscript writing. We thank Prof. Xu Zhang, Prof. Ayako Abe-Ouchi, Dr. Emma Boland, Dr. Feng He, and Dr. Takashi Obase for their very constructive discussions.

References

Abe-Ouchi, A., Saito, F., Kawamura, K., Raymo, M. E., Okuno, J., Takahashi, K., & Blatter, H. (2013). Insolation-driven 100,000-year glacial cycles and hysteresis of ice-sheet volume. *Nature*, *500*(7461), 190–193. https://doi.org/10.1038/nature12374

Akaike, H. (1973). Information theory and an extension of the maximum likelihood principle. In B. N. Petrov & F. Csaki (Eds.), *Proceedings of the 2nd international symposium on information theory* (pp. 267–281). Akademiai Kiado.

Barker, S., Diz, P., Vautravers, M. J., Pike, J., Knorr, G., Hall, I. R., & Broecker, W. S. (2009). Interhemispheric Atlantic seesaw response during the last deglaciation. *Nature*, *457*(7233), 1097–1102. https://doi.org/10.1038/nature07770

Barker, S., & Knorr, G. (2021). Millennial scale feedbacks determine the shape and rapidity of glacial termination. *Nature Communications*, *12*(1), 2273. https://doi.org/10.1038/s41467-021-22388-6

Barker, S., Lisiecki, L. E., Knorr, G., Nuber, S., & Tzedakis, P. C. (2025). Distinct roles for precession, obliquity, and eccentricity in Pleistocene 100-kyr glacial cycles. *Science*, *387*(6737), eadp3491. https://doi.org/10.1126/science.adp3491

Bereiter, B., Eggleston, S., Schmitt, J., Nehrbass-Ahles, C., Stocker, T. F., Fischer, H., et al. (2015). Revision of the EPICA Dome C CO_2 record from 800 to 600 kyr before present. *Geophysical Research Letters*, *42*(2), 542–549. https://doi.org/10.1002/2014GL061957

Böhm, E., Lippold, J., Gutjahr, M., Frank, M., Blaser, P., Antz, B., et al. (2015). Strong and deep Atlantic meridional overturning circulation during the last glacial cycle. *Nature*, *517*(7532), 73–76. https://doi.org/10.1038/nature14059

Boland, E. J. D., Atkinson, E., & Jones, D. (2023). A novel heuristic method for detecting overfit in unsupervised classification of climate models. *Environmental Data Science*, *2*, e46. https://doi.org/10.1017/eds.2023.40

Chaudhuri, P., & Marron, J. S. (1999). Sizer for exploration of structures in curves. *Journal of the American Statistical Association*, *94*(447), 807–823. https://doi.org/10.1080/01621459.1999.10474186

Clark, P. U., Dyke, A. S., Shakun, J. D., Carlson, A. E., Clark, J., Wohlfarth, B., et al. (2009). The last glacial maximum. *Science*, *325*(5941), 710–714. https://doi.org/10.1126/science.1172873

Clark, P. U., Shakun, J. D., Rosenthal, Y., Köhler, P., & Bartlein, P. J. (2024). Global and regional temperature change over the past 4.5 million years. *Science*, *383*(6685), 884–890. https://doi.org/10.1126/science.adi1908

Collins, L. G., Pike, J., Allen, C. S., & Hodgson, D. A. (2012). High-resolution reconstruction of southwest Atlantic sea-ice and its role in the carbon cycle during marine isotope stages 3 and 2. *Paleoceanography*, *27*(3), PA3217. https://doi.org/10.1029/2011PA002264

Cuffey, K. M., Clow, G. D., Steig, E. J., Buizert, C., Fudge, T. J., Koutnik, M., et al. (2016). Deglacial temperature history of West Antarctica. *Proceedings of the National Academy of Sciences of the United States of America*, *113*(50), 14249–14254. https://doi.org/10.1073/pnas.1609132113

Dempster, A. P., Laird, N. M., & Rubin, D. B. (1977). Maximum likelihood from incomplete data via the EM algorithm. *Journal of the Royal Statistical Society: Series B*, *39*(1), 1–22. https://doi.org/10.1111/j.2517-6161.1977.tb01600.x

Denton, G. H., Anderson, R. F., Toggweiler, J. R., Edwards, R. L., Schaefer, J. M., & Putnam, A. E. (2010). The last glacial termination. *Science*, *328*(5986), 1652–1656. https://doi.org/10.1126/science.1184119

Gregoire, L. J., Valdes, P. J., & Payne, A. J. (2015). The relative contribution of orbital forcing and greenhouse gases to the North American deglaciation. *Geophysical Research Letters*, *42*(22), 9970–9979. https://doi.org/10.1002/2015gl066005

Gu, S., Liu, Z., Oppo, D. W., Lynch-Stieglitz, J., Jahn, A., Zhang, J., & Wu, L. (2020). Assessing the potential capability of reconstructing glacial Atlantic water masses and AMOC using multiple proxies in CESM. *Earth and Planetary Science Letters*, *541*, 116294. https://doi.org/10.1016/j.epsl.2020.116294

He, F., & Clark, P. U. (2022). Freshwater forcing of the Atlantic Meridional Overturning Circulation revisited. *Nature Climate Change*, *12*(5), 449–454. https://doi.org/10.1038/s41558-022-01328-2

He, F., Shakun, J. D., Clark, P. U., Carlson, A. E., Liu, Z., Otto-Bliesner, B. L., & Kutzbach, J. E. (2013). Northern Hemisphere forcing of Southern Hemisphere climate during the last deglaciation. *Nature*, *494*(7435), 81–85. https://doi.org/10.1038/nature11822

Henry, L. G., McManus, J. F., Curry, W. B., Roberts, N. L., Piotrowski, A. M., & Keigwin, L. D. (2016). North Atlantic Ocean circulation and abrupt climate change during the last glaciation. *Science*, *353*(6298), 470–474. https://doi.org/10.1126/science.aaf5529

Hobart, B., Lisiecki, L. E., Rand, D., Lee, T., & Lawrence, C. E. (2023). Late Pleistocene 100-kyr glacial cycles paced by precession forcing of summer insolation. *Nature Geoscience*, *16*(8), 717–722. https://doi.org/10.1038/s41561-023-01235-x

Hu, T., Myers Toman, E., Chen, G., Shao, G., Zhou, Y., Li, Y., et al. (2021). Mapping fine-scale human disturbances in a working landscape with Landsat time series on Google Earth Engine. *ISPRS Journal of Photogrammetry and Remote Sensing*, *176*, 250–261. https://doi.org/10.1016/j.isprsjprs.2021.04.008

Huybers, P. (2006). Early Pleistocene glacial cycles and the integrated summer insolation forcing. *Science*, *313*(5786), 508–511. https://doi.org/10.1126/science.1125249

Huybers, P. (2011). Combined obliquity and precession pacing of late Pleistocene deglaciations. *Nature*, *480*(7376), 229–232. https://doi.org/10.1038/nature10626

Jones, D. C., Holt, H. J., Meijers, A. J. S., & Shuckburgh, E. (2019). Unsupervised clustering of Southern Ocean Argo float temperature profiles. *Journal of Geophysical Research: Oceans*, *124*(1), 390–402. https://doi.org/10.1029/2018jc014629

Jones, T. R., Roberts, W. H., Steig, E. J., Cuffey, K., Markle, B., & White, J. (2018). Southern hemisphere climate variability forced by northern hemisphere ice-sheet topography. *Nature*, *554*(7692), 351–355. https://doi.org/10.1038/nature24669

Laskar, J., Robutel, P., Joutel, F., Gastineau, M., Correia, A., & Levrard, B. (2004). A long-term numerical solution for the insolation quantities of the earth. *Astronomy and Astrophysics*, *428*(1), 261–285. https://doi.org/10.1051/0004-6361:20041335

Li, Y., Hu, T., Zhang, X., & Zhao, K. (2022). Rbeast: Bayesian change-point detection and time series decomposition [Software]. *GitHub release*. Retrieved from https://github.com/zhaokg/Rbeast/releases/tag/1.1.2.60

Liu, Z. (2023). Evolution of Atlantic meridional overturning circulation since the last glaciation: Model simulations and relevance to present and future. *Philosophical Transactions of the Royal Society A*, *381*(2262), 20220190. https://doi.org/10.1098/rsta.2022.0190

Marcott, S. A., Bauska, T. K., Buizert, C., Steig, E. J., Rosen, J. L., Cuffey, K. M., et al. (2014). Centennial-scale changes in the global carbon cycle during the last deglaciation. *Nature*, *514*(7524), 616–619. https://doi.org/10.1038/nature13799

Menviel, L., Spence, P., Yu, J., Chamberlain, M. A., Matear, R. J., Meissner, K. J., & England, M. H. (2018). Southern hemisphere westerlies as a driver of the early deglacial atmospheric CO_2 rise. *Nature Communications*, *9*(1), 2503. https://doi.org/10.1038/s41467-018-04876-4

Obase, T., Menviel, L., Abe-Ouchi, A., Vadsaria, T., Ivanovic, R., Snoll, B., et al. (2023). Multi-model assessment of the Deglacial climatic evolution at high southern latitudes. *Climate Past Discuss, 2023*, 1–45. https://doi.org/10.5194/cp-2023-86

Osman, M. B., Tierney, J. E., Zhu, J., Tardif, R., Hakim, G. J., King, J., & Poulsen, C. J. (2021). Globally resolved surface temperatures since the last glacial maximum. *Nature*, *599*(7884), 239–244. https://doi.org/10.1038/s41586-021-03984-4

Pedregosa, F., Varoquaux, G., Gramfort, A., Michel, V., Thirion, B., Grisel, O., et al. (2011). Scikit-learn: Machine learning in python. *Journal of Machine Learning Research*, *12*, 2825–2830.

Pedro, J. B., Jochum, M., Buizert, C., He, F., Barker, S., & Rasmussen, S. O. (2018). Beyond the bipolar seesaw: Toward a process understanding of interhemispheric coupling. *Quaternary Science Reviews*, *192*, 27–46. https://doi.org/10.1016/j.quascirev.2018.05.005

Pöppelmeier, F., Jeltsch-Thömmes, A., Lippold, J., Joos, F., & Stocker, T. F. (2023). Multi-proxy constraints on Atlantic circulation dynamics since the last ice age. *Nature Geoscience*, *16*(4), 349–356. https://doi.org/10.1038/s41561-023-01140-3

Pöppelmeier, F., Lippold, J., Blaser, P., Gutjahr, M., Frank, M., & Stocker, T. F. (2022). Neodymium isotopes as a paleo-water mass tracer: A model-data reassessment. *Quaternary Science Reviews*, *279*, 107404. https://doi.org/10.1016/j.quascirev.2022.107404

Praetorius, S. K., Condron, A., Mix, A. C., Walczak, M. H., McKay, J. L., & Du, J. (2020). The role of Northeast Pacific meltwater events in deglacial climate change. *Science Advances*, *6*(9), eaay2915. https://doi.org/10.1126/sciadv.aay2915

Praetorius, S. K., & Mix, A. C. (2014). Synchronization of North Pacific and Greenland climates preceded abrupt deglacial warming. *Science*, *345*(6195), 444–448. https://doi.org/10.1126/science.1252000

Roche, D. M., Renssen, H., Paillard, D., & Levavasseur, G. (2011). Deciphering the spatio-temporal complexity of climate change of the last deglaciation: A model analysis. *Climate of the Past*, *7*(2), 591–602. https://doi.org/10.5194/cp-7-591-2011

Sadatzki, H., Opdyke, B., Menviel, L., Leventer, A., Hope, J. M., Brocks, J. J., et al. (2023). Early sea ice decline off East Antarctica at the last glacial–interglacial climate transition. *Science Advances*, *9*(41), eadh9513. https://doi.org/10.1126/sciadv.adh9513

Seltzer, A. M., Ng, J., Aeschbach, W., Kipfer, R., Kulongoski, J. T., Severinghaus, J. P., & Stute, M. (2021). Widespread six degrees Celsius cooling on land during the last glacial maximum. *Nature*, *593*(7858), 228–232. https://doi.org/10.1038/s41586-021-03467-6

Shakun, J. D., & Carlson, A. E. (2010). A global perspective on last glacial maximum to Holocene climate change. *Quaternary Science Reviews*, *29*(15–16), 1801–1816. https://doi.org/10.1016/j.quascirev.2010.03.016

Shakun, J. D., Clark, P. U., He, F., Marcott, S. A., Mix, A. C., Liu, Z., et al. (2012). Global warming preceded by increasing carbon dioxide concentrations during the last deglaciation. *Nature*, *484*(7392), 49–54. https://doi.org/10.1038/nature10915

Snoll, B., Ivanovic, R., Gregoire, L., Sherriff-Tadano, S., Menviel, L., Obase, T., et al. (2024). A multi-model assessment of the early last deglaciation (PMIP4 LDv1): A meltwater perspective. *Climate of the Past*, *20*(4), 789–815. https://doi.org/10.5194/cp-20-789-2024

Spratt, R. M., & Lisiecki, L. E. (2016). A Late Pleistocene sea level stack. *Climate of the Past Discussions*, *12*(4), 1079–1092. https://doi.org/10.5194/cp-12-1079-2016

Stott, L., Timmermann, A., & Thunell, R. (2007). Southern hemisphere and deep-sea warming led deglacial atmospheric CO_2 rise and tropical warming. *Science*, *318*(5849), 435–438. https://doi.org/10.1126/science.1143791

Tierney, J. E., Zhu, J., King, J., Malevich, S. B., Hakim, G. J., & Poulsen, C. J. (2020). Glacial cooling and climate sensitivity revisited. *Nature*, *584*(7822), 569–573. https://doi.org/10.1038/s41586-020-2617-x

Timmermann, A., Timm, O., Stott, L., & Menviel, L. (2009). The roles of CO_2 and orbital forcing in driving southern hemispheric temperature variations during the last 21 000 yr. *Journal of Climate*, *22*(7), 1626–1640. https://doi.org/10.1175/2008jcli2161.1

van den Bos, V., Rees, A., Newnham, R., Vandergoes, M., Wilmshurst, J., & Augustinus, P. (2018). Holocene temperature, humidity and seasonality in northern New Zealand linked to southern hemisphere summer insolation. *Quaternary Science Reviews*, *201*, 77–88. https://doi.org/10.1016/j.quascirev.2018.10.008

WAIS Divide Project Members. (2013). Onset of deglacial warming in West Antarctica driven by local orbital forcing. *Nature*, *500*(7463), 440–444. https://doi.org/10.1038/nature12376

Wolff, E. W., Fischer, H., & Röthlisberger, R. (2009). Glacial terminations as southern warmings without northern control. *Nature Geoscience*, *2*(3), 206–209. https://doi.org/10.1038/ngeo442

Wu, Z., Yin, Q., Guo, Z., & Berger, A. (2020). Hemisphere differences in response of sea surface temperature and sea ice to precession and obliquity. *Global and Planetary Change*, *192*, 103223. https://doi.org/10.1016/j.gloplacha.2020.103223

Xuan, G., Zhang, W., & Chai, P. (2001). Em algorithms of Gaussian mixture model and hidden Markov model. In *Proceedings of the international conference on image processing*.

Ye, X., & Zhou, W. (2025). Unsupervised classification of global temperature profiles based on Gaussian mixture models. *Journal of Marine Science and Engineering*, *13*(1), 92. https://doi.org/10.3390/jmse13010092

Zhang, X., Barker, S., Knorr, G., Lohmann, G., Drysdale, R., Sun, Y., et al. (2021). Direct astronomical influence on abrupt climate variability. *Nature Geoscience*, *14*(11), 819–826. https://doi.org/10.1038/s41561-021-00846-6

Zhao, K., Valle, D., Popescu, S., Zhang, X., & Mallick, B. (2013). Hyperspectral remote sensing of plant biochemistry using Bayesian model averaging with variable and band selection. *Remote Sensing of Environment*, *132*, 102–119. https://doi.org/10.1016/j.rse.2012.12.026

Zhao, K., Wulder, M. A., Hu, T., Bright, R., Wu, Q., Qin, H., et al. (2019). Detecting change-point, trend, and seasonality in satellite time series data to track abrupt changes and nonlinear dynamics: A Bayesian ensemble algorithm. *Remote Sensing of Environment*, *232*, 111181. https://doi.org/10.1016/j.rse.2019.04.034